Journal of Power Sources 181 (2008) 79–84

Contents lists available at ScienceDirect

Journal of Power Sources

journal homepage: www.elsevier.com/locate/jpowsour

Short communication

Novel single step electrochemical route to γ-MnO_2 nanoparticle-coated polyaniline nanofibers: Thermal stability and formic acid oxidation on the resulting nanocomposites

G.K. Surya Prakash*, Palale Suresh, Federico Viva, George A. Olah

Loker Hydrocarbon Research Institute and Department of Chemistry, University of Southern California, 837 Bloom Walk, Los Angeles, CA 90089-1661, USA

ARTICLE INFO

Article history:
Received 4 January 2008
Received in revised form 29 February 2008
Accepted 3 March 2008
Available online 13 March 2008

Keywords:
γ-MnO_2 nanoparticle
Polyaniline (PANI) nanofibers
Conducting nanocomposites
Formic acid
Fuel cell
Electrooxidation

ABSTRACT

γ-MnO_2 nanoparticles-coated polyaniline (PANI) nanofibers on carbon electrode were prepared by potentiodynamic electrochemical deposition of PANI and MnO_2 from a single pot. Higher thermal stability of the resulting nanocomposites and their activity for formic acid oxidation permits the realization of a platinum-free anode for formic acid fuel cells.

1. Introduction

Polyaniline (PANI) is one of the most promising conducting polymers due to its ease of preparation and good environmental stability combined with moderate electrical conductivity [1]. The wide range of associated electrical, electrochemical and optical properties makes polyaniline potentially attractive for applications as a synthetic metal [2]. Heightened interest in one-dimensional electrical conductors and the need to produce nanoscale electrical circuits has prompted recent research to focus on polyaniline nanofibers [3–5]. More recently, different methods have been reported for the synthesis of polyaniline nanofibers without using any templates since template removal is tedious, particularly when hard templates are utilized [6]. Techniques such as interfacial polymerization [7], nanofiber seeding [8] and radiolysis [6] have been developed.

Manganese oxides have long been known as materials of technological importance for catalytic and electrochemical applications [9]. MnO_2 is a promising material because it is inexpensive, safe and environmentally friendly. MnO_2 is known to exist in a wide variety of structural forms, such as α-, β-, γ- and δ-types [10]. Among these phases, γ-phase is known to be electrochemically most active and most of the electrochemically synthesized MnO_2 is in the γ-phase [11,12].

Conducting polymer nanocomposites containing metal oxides have attracted a great deal of interest from researchers because they frequently exhibit unexpected hybrid properties, synergically derived from both components [13]. Enhanced conductivity and special mechanical, electrochemical, optical, magnetic as well as thermal properties of these composites make them promising materials. In this area, new PANI/inorganic nanocomposites are also triggering increased interests from both academic and industrial scientists. Many PANI/inorganic nanocomposites, such as PANI/TiO_2, PANI/ZrO_2, PANI/Fe_3O_4, PANI/TiN, PANI/V_2O_5 and PANI/ZnO have been reported in the literature [14–19]. In all these reports, either in situ chemical polymerization techniques or electrochemical polymerization of PANI followed by dipping the partially oxidized PANI in a suspension of the metal oxide is reported for the synthesis of composites. However, in all these methods, some amount of free oxide particles are seen, which affect the electrochemical and thermal properties of these composites greatly. To the best of our knowledge there are no single step electrochemical routes known for the synthesis of PANI/inorganic oxide composites in the literature.

Even though PANI is found to be thermally stable up to 200 °C, PANI films were found to loose their conductivity and electrochemical properties, when heated at 80 °C for a prolonged period of

* Corresponding author. Tel.: +1 213 740 5984; fax: +1 213 740 6270.
E-mail address: gprakash@usc.edu (G.K.S. Prakash).

0378-7753/$ – see front matter © 2008 Elsevier B.V. All rights reserved.
doi:10.1016/j.jpowsour.2008.03.007

time [20]. Hence, even though there are reports on the catalytic activity of PANI in the reactions of anodic oxidation of hydrogen [21], methanol [22] and ascorbic acid [23], there are no studies that report a fuel cell full membrane electrode assembly (MEA), using PANI. The main advantage of fuel cells employing liquid organic fuels as compared to those using hydrogen is the simplicity of fuel storage, dispense and recharging. Among the fuel cells with liquid fuels, the most thoroughly studied are fuel cells with direct methanol and direct formic acid oxidations. The advantage of formic acid fuel cell compared to methanol is the simple reaction nature and lower extent of fuel crossover through the proton conducting membrane [24]. In general, the anode and cathode of the fuel cells are electrodes with catalyst coatings, which are usually platinum based. The limited resource of this metal on the earth and cost has stimulated interest in developing non-platinum based catalysts. With this in mind, we report a novel single step electrochemical method for the synthesis of γ-MnO_2 nanoparticle-coated PANI nanofibers on carbon electrodes by potentiodynamic electrochemical deposition of PANI and MnO_2. Higher thermal stability of the resulting nanocomposite and its activity for formic acid oxidation allowed us to realize a platinum-free anode for formic acid fuel cells.

2. Materials and methods

2.1. Materials

Aniline 99.5%, formic acid >96% and Nafion ionomer solution (5% in alcohol) were purchased from the Aldrich. Sulphuric acid was supplied by EMD chemicals. Analytical grade $MnSO_4{\cdot}2H_2O$ was used. Alfa Aesar supplied the Pt black powder HiSPEC 1000 catalyst. All solutions were made using Milli-Q deionized water from a Millipore Direct-Q3 system.

2.2. Synthesis of PANI/MnO_2 composite

Non-teflonised carbon (Toray paper of area 1.6 cm^2) was employed as the working electrode. Electrochemical cell was a glass container, which had a provision to introduce the working electrode, Pt counter electrode (2 cm^2) and a reference electrode. Reference electrode used was the standard calomel electrode (SCE). It is known that the quality of the PANI films deposited by potentiodynamic method is better than the films obtained by potentiostatic or galvanostatic methods [25]. Hence a potentiodynamic method was employed for the preparation of PANI/MnO_2 composites. An electrolyte solution of 0.5 M H_2SO_4 with 0.5 M aniline was employed for PANI synthesis and a solution of 0.5 M H_2SO_4 with 0.5 M aniline and 0.5 M $MnSO_4{\cdot}2H_2O$ was employed for the composite synthesis. PANI or PANI/MnO_2 was deposited over 10 cycles. After deposition, the electrodes were washed three times using Milli-Q deionized water in an ultrasonic bath. For the thermal studies, the electrodes were prepared as mentioned and heated in air at 90 °C for 36 h.

2.3. Composite characterization

XRD patterns of the PANI and PANI/MnO_2 composites were recorded using powder diffraction instrument, Rigaku X-ray diffractometer, with Cu Kα at a scan rate of 1 min^{-1}. FTIR spectra of the fabricated and heat-treated PANI and PANI/MnO_2 composites were recorded using Perkin and Elmer FTIR spectrometer, 250 scans per spectrum at 4 cm^{-1} resolution in the wavelength range 650–4000 cm^{-1}. Scanning electron microscopic images were captured using a Cambridge 360 scanning electron microscope.

Cyclic voltammetry and electrochemical impedance spectroscopy (EIS) measurements were performed with a Solartron SI 1287 and SI 1260 Impedance-Phase Analyzer. Glass cell, reference electrode and counter electrode were the same as used in Section 2.2. CVs were performed in 0.5 M H_2SO_4 sweeping at 10 mV s^{-1} for 10 cycles between −0.2 and 0.8 V vs. SCE for the characterization of PANI and PANI/MnO_2 and PANI/MnO_2 in 0.5 M H_2SO_4 + 0.5 M HCOOH for formic acid oxidation. EIS was used to determine the resistance of the electrode before and after annealing. Measurements were recorded in 0.5 M H_2SO_4 at open circuit voltage with 10 mV of amplitude. Real impedance value, when the imaginary impedance is zero, corresponds to the cell ohmic resistance. The difference in ohmic resistance before and after annealing is attributed to a change in PANI or PANI/MnO_2 as the other components of the cell do not change.

2.4. Fuel cell preparation and assembly

PANI/MnO_2 was deposited on the one side of the carbon paper of dimensions 6 cm × 6 cm using the method described in Section 2.2. To prevent the deposition on both sides, the carbon paper was pasted to a MMA sheet using a dielectric tape to expose only an area of 25 cm^2. The whole setup was dipped into the aniline or aniline/$MnSO_4$ solution during deposition. After the deposition, the electrode was removed from the MMA sheet and the borders were cut to obtain PANI or PANI/MnO_2 deposited on a 25 cm^2 carbon paper electrode.

A Nafion membrane cut in the dimension of 8 cm × 8 cm was pretreated by boiling in a solution of 5% H_2O_2 and 1 M H_2SO_4 at 80 °C for 20 min and was washed several times with deionized water. Cathode ink was prepared by mixing Pt catalyst (8 mg cm^{-2}), water and a Nafion ionomer solution in 1:3:1 wt% and is painted uniformly on to the carbon. The cathode and anode were then pressed on either side of Nafion 117 membrane with 250 kg force at 120 °C for 1 h. Fuel cell was assembled using this MEA, vide supra, by inserting it in between two graphite blocks for current collection. Two 0.5 mm thick Teflon gaskets were introduced between the electrodes and the carbon blocks. A uniform torque of 36 N m^{-1} was applied to each bolt used to assemble the cell. Cell was conditioned overnight by passing water on both sides. For testing the fuel cell, 0.5 M HCOOH with a small amount of 0.5 M sulphuric acid was passed to the anode side at a constant rate and O_2 to the cathode at a rate of 30 ml min^{-1} at ambient pressure. The fuel cell performance was evaluated using the Fuel cell test system Series 890B from Scribner Associates, Inc. by galvanodynamic scans from 0 A with increments of 0.5 A every 90 s to provide polarization plots. From these plots, power densities were calculated by multiplying voltage times current density. The experiments were conducted at three different temperatures of 30, 60 and 80 °C, respectively.

3. Results and discussion

3.1. PANI/MnO_2 synthesis and characterization

Single step synthesis of the PANI/MnO_2 composite was performed by sweeping the carbon electrode voltage between −0.2 and 1.35 V vs. SCE using a solution containing 0.5 M H_2SO_4, 0.5 M aniline and 0.5 M $MnSO_4{\cdot}2H_2O$. When the potential is scanned in the anodic direction, upon reaching 1.2 V vs. SCE, electropolymerization of aniline takes place resulting in the formation of polyaniline fibers. On further increase of potential up to 1.35 V vs. SCE, MnO_2 is formed on the previously formed polyaniline according to the following half reaction:

$$Mn^{2+} + 2H_2O \rightarrow MnO_2 + 4H^+ + 2e^- \quad (1)$$

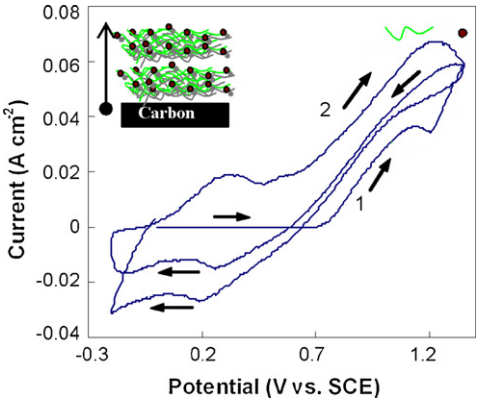

Fig. 1. First two voltammogram cycles for the synthesis of PANI/MnO_2 composite at a scan rate of 50 mV s^{-1}. The squiggle ( ) at 1.2 V represents the PANI formation region and the dot ( ) at 1.35 V wherein the MnO_2 nanoparticles are formed. Inset shows the schematic representation for the structure of the PANI/MnO_2 composite.

The electrode fabrications were performed at three different sweep rates: 10, 50 and 100 mV s^{-1}. Fig. 1 shows the first two cycles for the single step process sweeping at 50 mV s^{-1}. This process was repeated during the subsequent cycles resulting in PANI/MnO_2 nanocomposites. The difference in the weights of PANI and PANI/MnO_2 deposited after 10 cycles gives the weight ratio of PANI to MnO_2 as 70:30%. Morphology (SEM images) of the PANI only samples synthesized by potentiodynamic method by scanning the potential of the carbon electrode between −0.2 and 1.2 V vs. SCE at different scan rates of 10, 50 and 100 mV s^{-1} and that of the bare carbon electrode are shown in Fig. 2. When the scan rate of deposition is 10 mV s^{-1}, we obtain PANI films, which are formed by the agglomerated PANI nanoparticles of size ranging between 400 and 500 nm. On increasing the scan rate to 50 mV s^{-1}, we obtain PANI nanofibers with average diameter of 50 nm and no free nanoparticles are seen. When the scan rate of deposition is 100 mV s^{-1}, we see the PANI nanofibers with large number of PANI nanoparticles attached to them. Hence it is clear that there is an optimum rate of formation of PANI, which results in PANI nanofibers. Hence the scan rate of deposition plays an important role in the resulting PANI morphology.

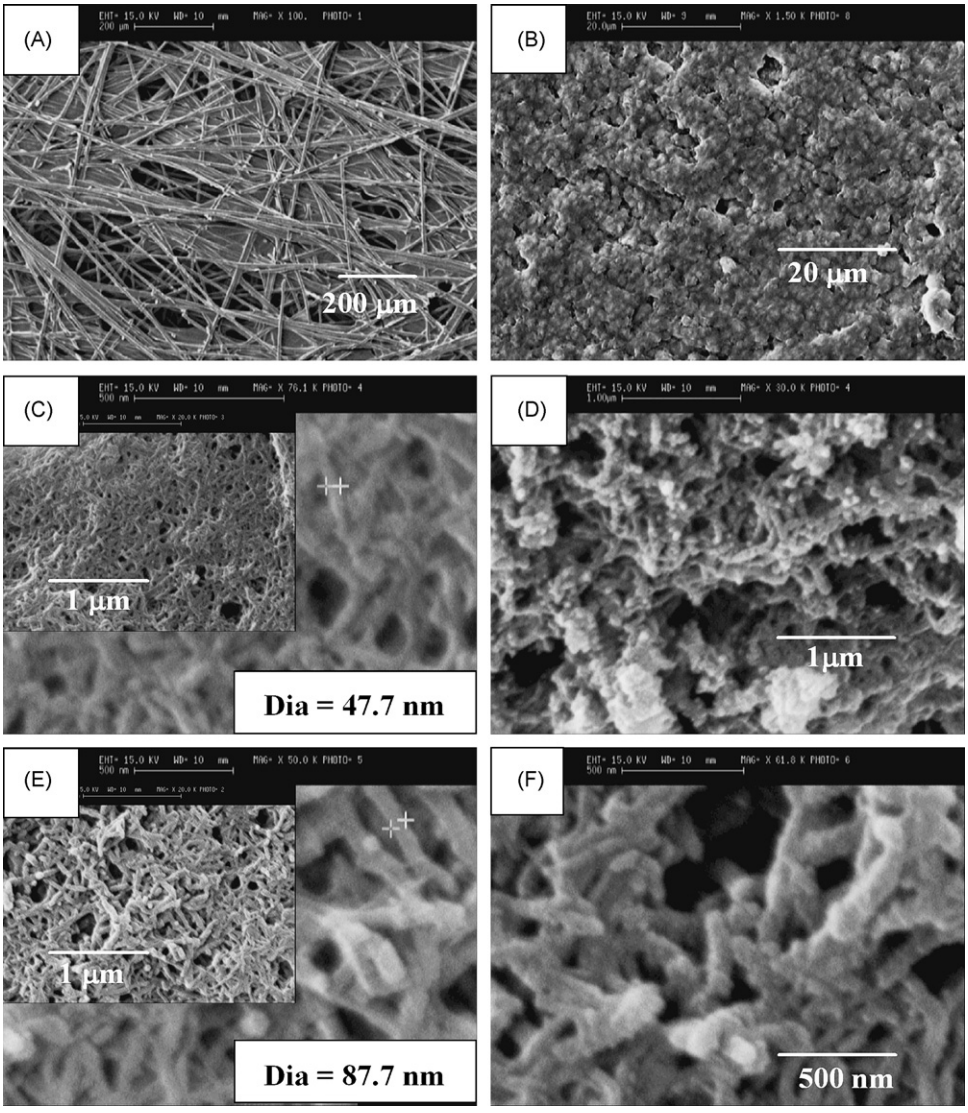

Fig. 2. SEM images: (A) carbon paper, (B–D) PANI deposition at 10, 50 and 100 mV s^{-1}, respectively, and (E and F) PANI/MnO_2 nanocomposite deposited at 50 mV s^{-1}.

Reasons for this kind of morphology change with the scan rate of deposition are quite complex. Nanofiber seeding method is reported for the synthesis of polyaniline nanofibers [8]. The authors observed that the nanoscale morphology of the seed fiber is transcribed over many length scales in the resulting polyaniline nanofibers and there is an influence of inert surfaces (walls of the reaction flask, etc.) on progress of the reaction. Although the general shape of the seed appeared to control the overall morphology of the fibers, specific differences in the length, diameter, etc., of the seeds did not appear to have a significant impact. Based on the above facts, the possible explanation for the morphology change may be given as follows. SEM image of the carbon electrode used for the deposition is shown in Fig. 2(A). The paper is made up of several carbon fibers. When the cycling scan rate is low, growing of PANI polymer is slow and deposition takes place more uniformly and the underlying carbon substrate does not direct the morphology of the polymer formed. When the scan rate is increased to 50 mV s^{-1}, PANI growth is faster and the underlying carbon fibers direct the growth of the forming polyaniline acting like seeds, which can control the morphology of the forming PANI as reported [8]. With further increase in scan rate, the growth of PANI polymer is even faster and hence along with nanofibers some nanoparticles are also formed. The change in morphology of the PANI formed at different scan rates on carbon paper opens up a new simple route for a synthesis of thin, substrate-supported polyaniline nanofibers without requiring any bulk processing step.

Morphology of the PANI/MnO_2 nanocomposite synthesized by the potentiodynamic method at a scan rate of 50 mV s^{-1} is shown in Fig. 2(E and F). MnO_2 nanoparticles of about 40 nm size are found to decorate the previously formed PANI nanofibers on both sides and the diameter of the fiber is found to be doubled (≈87 nm). PANI and PANI/MnO_2 composite are characterized by FTIR spectroscopy and XRD and the representative results are shown in Fig. 3. To characterize PANI and to understand the interaction between MnO_2 nanoparticles and PANI, we preferentially used FTIR spectroscopy. The IR spectra of the PANI and PANI/MnO_2 nanocomposite are shown in Fig. 3(A). FTIR PANI spectra shows that the PANI is in the emeraldine form. Bands at 1623 and 1506 cm^{-1} corresponds to the C=C stretching of quinoid rings and C=C stretching of the benzenoid rings, respectively. The bands in the range 1200–1400 cm^{-1} are the C–N stretching band of the aromatic amine. The weak band at 3320 cm^{-1} is attributed to N–H stretching. The strong band at 1195 cm^{-1} was described by MacDiarmid and co-workers [26] as the "electronic-like band" and is considered to be a measure of the degree of delocalization of electrons and thus a characteristic peak of PANI conductivity and the peak at 835 cm^{-1} for the out-of-plane bending of the C–H bond. As commonly observed for emeraldine salt polyaniline, the quinoid band at 1600 cm^{-1} is less intense than that of the benzenoid band at 1500 cm^{-1}. But here, we observe an inverse in the 1600/1500 cm^{-1} intensity ratios. The data reveal that the PANI synthesized here is richer in quinoid units rather than benzenoid forms. This may be due to the interaction of carbon fibers of the carbon electrodes used for PANI deposition, which promote and stabilize the quinoid ring structures as observed in the case of multiwalled carbon nanotubes/PANI composites [27]. This further supports our explanation for PANI fiber formation. FTIR spectra of the PANI/MnO_2 composite is similar to that of PANI, but the intensity of the band at 1195 cm^{-1} is much higher indicating higher conductivity for the composite. The band at 3320 cm^{-1} is lower in intensity and also shifts slightly to higher values indicating the perturbation of the H-bonding environment.

In the X-ray diffraction pattern (Fig. 3(B)), intense peaks are observed for the carbon substrate at $2\theta = 26^\circ$ and 55° with some less intense peaks. XRD pattern of PANI nanofiber electrode shows intense peak centered at $2\theta = 25^\circ$ due to the periodicity parallel to

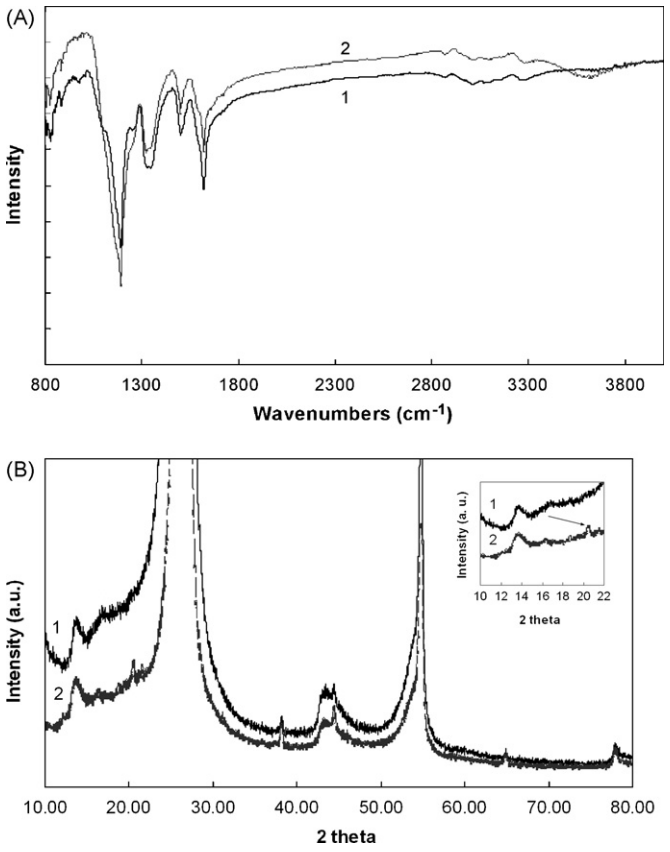

Fig. 3. (A) FTIR spectra and (B) XRD patterns for PANI (1) and PANI/MnO_2 composite (2). Inset in (B) shows the expansion of the XRD patterns for PANI and PANI/MnO_2 composite in the 2θ range of 10–22°. Arrow indicates $2\theta = 20^\circ$ peak corresponding to γ-MnO_2.

the polymer chain and some weak peaks at lower angles and the pattern is similar to that reported for the PANI/emeraldine salt. XRD pattern of PANI/MnO_2 composite shows an extra intense peak at $2\theta = 20^\circ$, shown on inset in Fig. 3(B) by an arrow, and can be assigned to γ-MnO_2. Generally, electrochemical synthesis of MnO_2 in acidic medium gives amorphous γ-MnO_2 as observed from earlier studies. Thermal stability of the PANI and PANI/MnO_2 are studied by heating the samples at 90 °C for 36 h. FTIR spectra and cyclic voltammogram of the samples before and after annealing were obtained. The degradation of the films doped by acids is well documented by the changes in the spectra observed at wave numbers below 2000 cm^{-1}. These changes correspond to deprotonation during the thermal annealing of the films. In Fig. 4, the FTIR spectra before and after annealing are shown. In the PANI spectra (Fig. 4(A)), the bands characteristic of polymer backbone at 1500 and 1600 cm^{-1} are shifted to higher values after annealing indicating the deprotonation, whereas the values are almost same for the composites (Fig. 4(B)). The peak at 1195 cm^{-1} is suppressed after annealing to a grater extent for PANI compared to that of the composites, indicating higher extent of deprotonation in pure PANI compared to the composites. However, the behavior of the composite obtained by depositing PANI and MnO_2 from two different pots in two stages is similar to that of pure PANI indicating the importance of homogenous distribution of PANI and MnO_2 nanoparticles for the higher stability.

Cyclic voltammograms of the PANI before and after annealing clearly show many differences as seen in Fig. 5(A and B). In Fig. 5(A), the peak at 0.25 V in the anodic direction, which corresponds to the leucoemeraldine to emeraldine transition, is shifted to higher

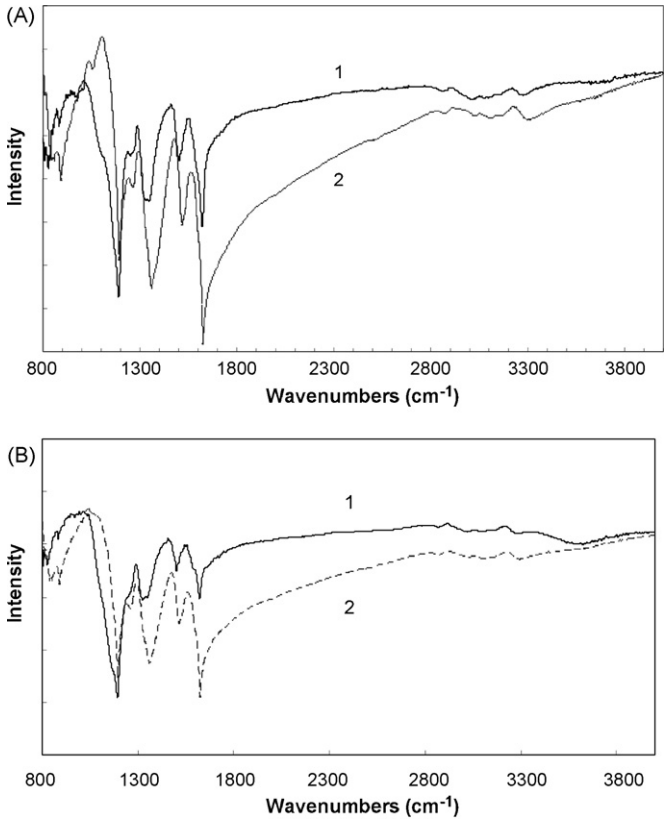

Fig. 4. FTIR spectra for PANI (1) and PANI/MnO_2 composite (2): (A) before and (B) after annealing.

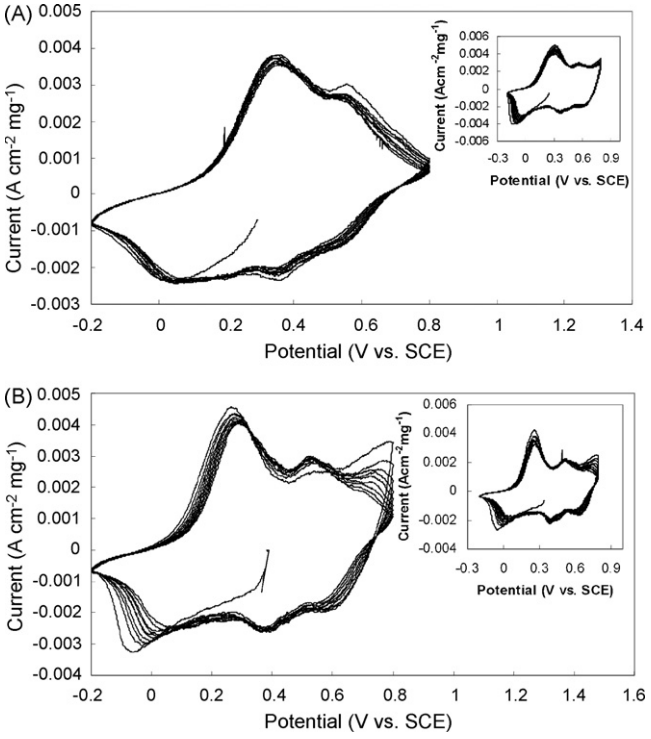

Fig. 5. Cyclic voltammograms for the annealed PANI (A) and PANI/MnO_2 (B) composite in 0.5 M H_2SO_4 at a scan rate of 10 mV s^{-1}. Insets in (A) and (B) shows respective cyclic voltammograms before annealing.

potential and the peak at 0.7 V, which corresponds to the emeraldine to pernigraniline transition shifts to lower potentials. Peak currents also decrease considerably. However, the cyclic voltammogram of the annealed PANI/MnO_2 composite (Fig. 5(B)) shows no shift in peaks compared to the sample before annealing, nor in the current density values for those peaks, giving another indication on the thermal stability of the composite. The polymer degrades when it is cycled repeatedly and this is indicated in the voltammograms by the decreasing current. It appears that the extent of the degradation by cycling is higher in the composite. This is most likely due to the reduction of MnO_2 and detachment from the composite. The suppression of the 1195 cm^{-1} band for PANI compared to PANI/MnO_2 after annealing agrees with the resistance value measured by EIS. For PANI there is an increase of the resistance by a factor of 2 while the resistance of PANI/MnO_2 does not change.

Cyclic voltammograms of the PANI/MnO_2 composites in 0.5 M H_2SO_4 and 0.5 M H_2SO_4 and 0.5 M HCOOH mixtures were recorded. As Fig. 6 shows, the voltammogram shape does not change and only an increase in the peak current densities can be noticed for the 0.5 M H_2SO_4 and 0.5 M HCOOH mixture. Even though the voltammogram does not show a clear activity for formic acid oxidation, MEAs were assembled and tested.

3.2. Single cell fuel cell testing

Performance of the fuel cell using MEAs with the PANI/MnO_2 deposited on Toray carbon paper as an anode and Pt deposited on carbon as a cathode and a Nafion 117 membrane were studied. The anode electrodes were obtained using the process described in Section 2.2 with a sweeping rate of 50 mV s^{-1}. This was considered to be the optimum sweep rate. After performing the deposition for 10 cycles, the composite loading on the electrode was 12 mg cm^{-2}. Fig. 7 shows a scheme detailing the MEA setup.

The fuel cell assembled showed an open circuit voltage of 550 mV. This was an indication that the oxidation of formic acid was taking place. Subsequently, galvanodynamic measurements were carried out as described in Section 2.4. The polarization plots and the power densities calculated can be seen in Fig. 8(A). Power densities of 3, 5 and 12 mW cm^{-2} were obtained at 30, 60 and 80 °C, respectively. Liberated gases from the anode were analyzed using GC and carbon dioxide was the only product observed and no carbon monoxide was detected. Possible mechanism of formic

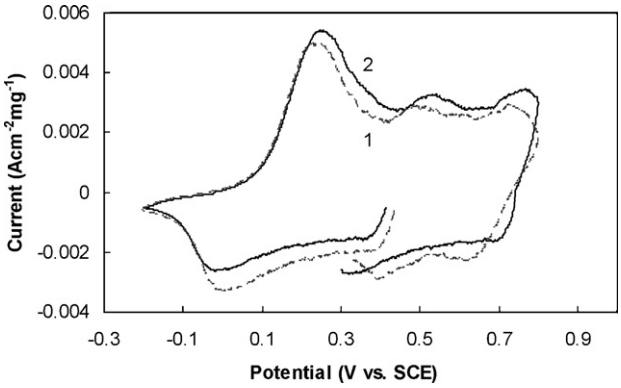

Fig. 6. Cyclic voltammograms for the PANI/MnO_2 composite in 0.5 M H_2SO_4 (1) and 0.5 M H_2SO_4 and 0.5 M HCOOH (2) at a scan rate of 10 mV s^{-1}.

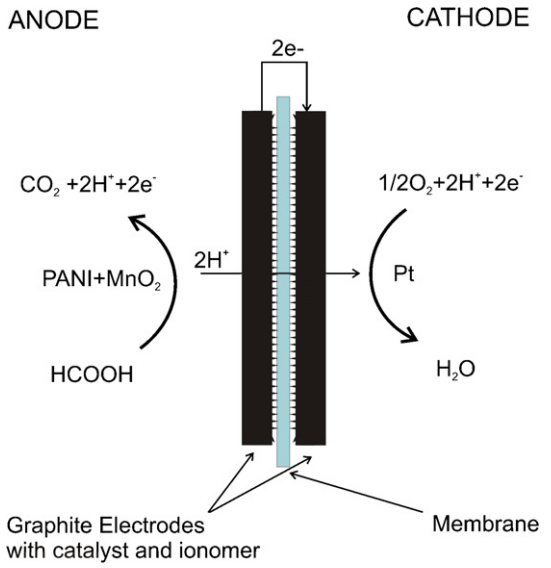

Fig. 7. MEA for the formic acid fuel cell.

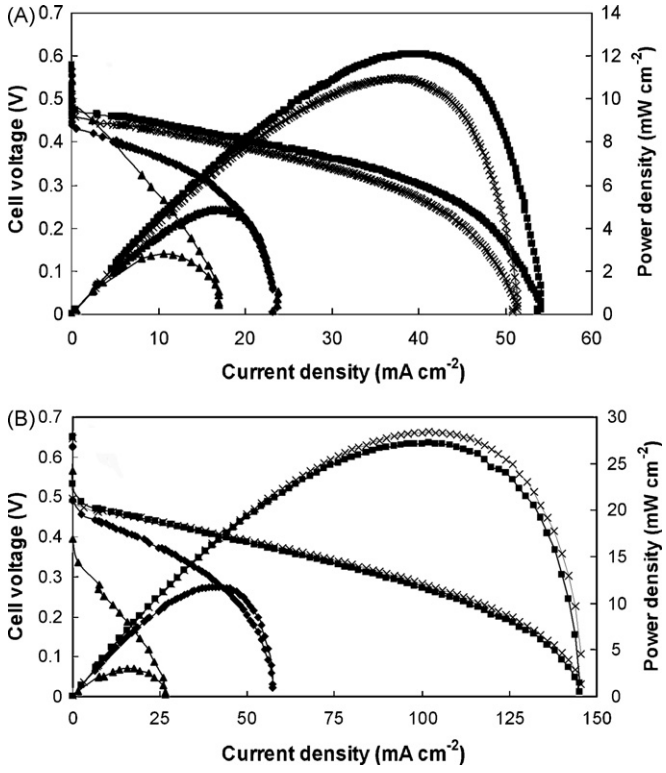

Fig. 8. Polarization and power densities plot comparison of (A) as synthesized and (B) electrode kept at 250 mV in 0.5 M H_2SO_4, in a formic acid fuel cell at (▲) 30 °C, (♦) 60 °C and (■) 80 °C. The (+) data shows the second day performance at 80 °C.

acid oxidation by PANI/MnO_2 composite may be the reduction of PANI from the emeraldine form to leucoemeraldine form, which is accompanied by the formic acid oxidation and in turn is followed by leucoemeraldine oxidation to emeraldine and electron transfer to the anode. If this is the case, then higher amount of PANI in emeraldine form should result in higher activity for the formic acid oxidation. The fabricated sample of PANI should contain a mixture of leucoemeraldine and emeraldine forms since the end potential used during the deposition is 0 V. We kept the PANI/MnO_2 film at 250 mV in H_2SO_4 until the current falls to zero so that most of the PANI stays in the emeraldine form and such an electrode was then assembled in a fuel cell. Performance of this fuel cell is shown in Fig. 8(B). Power density values obtained were higher at 3.5, 11 and 26 mW cm^{-2} at 30, 60 and 80 °C, respectively. Better performance of this cell compared to the former seems to support the above-stated mechanism.

4. Conclusions

Potentiodynamic synthesis of PANI/MnO_2 composite in a single pot was developed. SEM images show the change in morphology with CVs sweep rate during synthesis, giving a tool to obtain composites with controlled size of fiber and particles. From the FTIR characterization data it can be stated that PANI in our composites are richer in quinoid units, presenting higher conductivity, and that the extent of deprotonation after annealing is lower for the composite than for the pure PANI, corroborated by the resistance measurement of the PANI and composites by a.c. impedance.

Finally, the composites show good activity as oxidation catalysts for formic acid in fuel cells, as can be seen in Fig. 8(A and B) from the polarization and power density plots. The emeraldine content in the PANI/MnO_2 anode catalyst appears to be important for better performance of the fuel cell.

Acknowledgment

Support of our work by the Stauffer Foundation is gratefully acknowledged.

References

[1] A.G. MacDiarmid, J.C. Chiang, M. Haipern, W.S. Huang, S.L. Mu, N.L. Somasiri, W. Wu, S.I. Yaniger, Mol. Cryst. Liq. Cryst. 121 (1985) 173.
[2] K.G. Neoh, E.T. Kang, K.L. Tan, Polymer 33 (1992) 2292.
[3] C.G. Wu, T. Bein, Science 264 (1994) 1757.
[4] C.R. Martin, Science 266 (1994) 1961.
[5] J.C. Chiang, A.G. MacDiarmid, Synth. Met. 13 (1986) 193.
[6] S.K. Pillalamarri, F.D. Blum, A.T. Tokuhiro, J.G. Story, M.F. Bertino, Chem. Mater. 17 (2005) 227.
[7] J. Huang, R.B. Kaner, J. Am. Chem. Soc. 126 (2004) 851.
[8] X. Zhang, W.J. Goux, S.K. Manohar, J. Am. Chem. Soc. 126 (2004) 4502.
[9] H.Y. Lee, G.B. Goodenough, J. Solid State Chem. 144 (1999) 220.
[10] M.H. Huang, S. Mao, H. Feick, H. Yan, Y. Wu, H. Kind, E. Weber, R. Russo, P. Yang, Science 292 (2001) 1897.
[11] J.M. Tarascon, Mater. Technol. 8 (1993) 39.
[12] S. Rodrigues, N. Munichandraiah, A.K. Shukla, J. Appl. Electrochem. 28 (1998) 1235.
[13] A. Maity, M. Biswas, J. Appl. Polym. Sci. 94 (2004) 803.
[14] K. West, T. Jacobsen, B. Zachau-Christaiansen, M.A. Careem, S. Skaarup, J. Power Sources 43 (1993) 127.
[15] S. Wang, Z. Tan, Y. Li, L. Sun, T. Zhang, Thermochim. Acta 441 (2006) 191.
[16] J. Deng, C. He, Y. Peng, J. Wang, X. Long, P. Li, A.S.C. Chan, Synth. Met. 139 (2003) 295.
[17] Y. Qiu, L. Gao, J. Phys. Chem. B 109 (2005) 19732.
[18] M.L. Cantu, P.G. Romero, J. Electrochem. Soc. 146 (1999) 2029.
[19] Z.X. Zheng, Y.Y. Xi, H.G. Huang, L.L. Wu, Z.H. Lin, Phys. Chem. Comm. 1 (2001) 21.
[20] S.K. Mondal, N. Munichandraiah, J. Electroanal. Chem. 78 (2006) 595.
[21] C. Chen, C. Bose, K. Rajeshwar, J. Electroanal. Chem. 161 (1993) 350.
[22] K. Kost, D. Bartak, Anal. Chem. 80 (1998) 2379.
[23] S.K. Mondal, R.K. Raman, A.K. Shukla, N. Munichandraiah, J. Power Sources 145 (2005) 16.
[24] C. Rice, S. Ha, R.I. Masel, J. Power Sources 111 (2002) 83.
[25] S.K. Mondal, K.R. Prasal, N. Munichandraiah, Synth. Met. 148 (2005) 275.
[26] S. Quillard, G. Louarn, S. Lefrant, A.G. MacDiarmid, Phys. Rev. B 50 (1994) 12496.
[27] H. Zengin, W. Zhou, J. Jin, R. Czerw, D.W. Smith, L. Echegoyen, D.L. Carroll, S.H. Foulger, J. Ballato, Adv. Mater. 14 (2002) 1480.